


**Elusive isolating frequency of a locally resonant mechanical meta-layer**Yunhao Zhang,<sup>1</sup> Hao Zhou,<sup>2</sup> and Yongquan Liu <sup>1,3,\*</sup><sup>1</sup>*State Key Laboratory for Strength and Vibration of Mechanical Structures, School of Aerospace Engineering, Xi'an Jiaotong University, Xi'an 710049, China*<sup>2</sup>*Beijing Institute of Spacecraft System Engineering, China Academy of Space Technology, Beijing 100094, China*<sup>3</sup>*National Key Laboratory of Science and Technology on Liquid Rocket Engines, Xi'an 710100, China*

(Received 13 May 2023; revised 28 July 2023; accepted 6 October 2023; published 19 October 2023)

In this work, we report a meta-layer consisting of subwavelength local resonators to achieve low-frequency isolation of elastic waves. Apart from its distinctive low-dimensional configuration with a thickness of  $\frac{1}{7}$  the wavelength, the meta-layer differs from bandgap-based metamaterials in that its optimally isolating frequency is higher than the eigenfrequency. We demonstrate theoretically, numerically, and experimentally that the isolating frequency shift arises from the coupling effect between the resonators and the load-carrying plate or beam. As a further step, to demonstrate the universality of our theory, we predict and design a meta-layer with an opposite-frequency shift. The proposed meta-layer, along with its corresponding theory, can precisely guide the development of compact low-frequency wave isolation devices.

DOI: [10.1103/PhysRevB.108.L140303](https://doi.org/10.1103/PhysRevB.108.L140303)

The manipulation of guided waves in solids is a critical issue for applications such as structural vibration control, energy harvesting, and nondestructive testing [1,2]. Elastic metamaterial, an artificial structure composed of periodic sub-wavelength units, provides a powerful tool for the control of elastic waves, enabling plenty of functions, such as negative refraction [3–5], cloaking [6,7], and backscattering immune waveguides [8,9]. One of the most promising applications is isolation of elastic waves. In 2000, the sonic metamaterial based on local resonance was first proposed to isolate long-wavelength acoustic waves by using tiny structures [10]. It was further studied that the locally resonant bandgap is due to the negative equivalent mass of units at eigenfrequency [11–13]. Subsequently, locally resonant metamaterials are rapidly applied to beams [14–16] and plates [17,18] for elastic wave isolation and vibration control. However, a bulky size with at least several wavelengths is always required to satisfy the periodic arrangement of abundant units, which poses challenges in structure fabrication and limits their practical engineering applications.

Recently, the advent of a metasurface, a monolayer structure composed of meticulously designed subwavelength units, provides a new perspective to solve the size-related challenge [19,20]. The metasurface was soon introduced into elastic wave manipulation due to its compact configuration, achieving anomalous refraction [21–24], focusing [25–27], source camouflage [28,29], and asymmetric transmission [30,31] via phase and amplitude discontinuities. As for isolation of elastic waves, existing metasurfaces are still in their infancy. Generally speaking, elastic wave isolation can be achieved by phase-shift modulation based on the generalized Snell's law [20,32], which leads to an insolvable transmission angle  $\theta$ ,

[33,34]. We proposed a distinct method of isolation through the coherent cancellation of scattered and incident waves, and further designed an omnidirectionally isolating interface in a broad frequency band from 3 to 7 kHz [35]. Nonetheless, vibration isolation and absorption are predominantly desirable in the low-frequency range of less than 1 kHz [36–38]. Considering that the working frequency of presented metasurfaces is excessively high for practical engineering applications [39], the development of a compact method that can effectively isolate low-frequency elastic waves remains a significant challenge [40,41].

Regarding the feasibility of developing locally resonant metamaterials for low-frequency isolation, we designed a meta-layer consisting of subwavelength local resonators to isolate low-frequency elastic waves. The isolation performance is verified by experiments and simulations, in which we observed that the isolating frequency is higher than the unit's eigenfrequency. We prove that the isolating frequency shift is caused by the coupling between the resonator and the load-bearing structure. In addition, we further design a meta-layer with an opposite-frequency shift, showing the universality of our theory. The proposed meta-layer distinguishes itself from conventional locally resonant metamaterials, providing precise design guidelines for the development of compact devices for low-frequency isolation.

As shown in Fig. 1(a), the unit of a low-frequency isolating meta-layer consists of a mass block and a cantilever beam. Its material properties and geometric size are provided in Supplemental Material Appendix S1 [42]. The block and the curved beam are considered mass and spring, respectively, forming a mass-spring system with eigenfrequency  $\omega_0 = 2\pi f_0$ . The eigenfrequency of the designed unit is tested by experiments, where the unit is fixed on a metal pedestal and excited by a vibration generator. Experimental results are shown in Fig. 1(b), in which  $w_A$  and  $w_B$  refer to the displacement on

\*liuy2018@xjtu.edu.cn

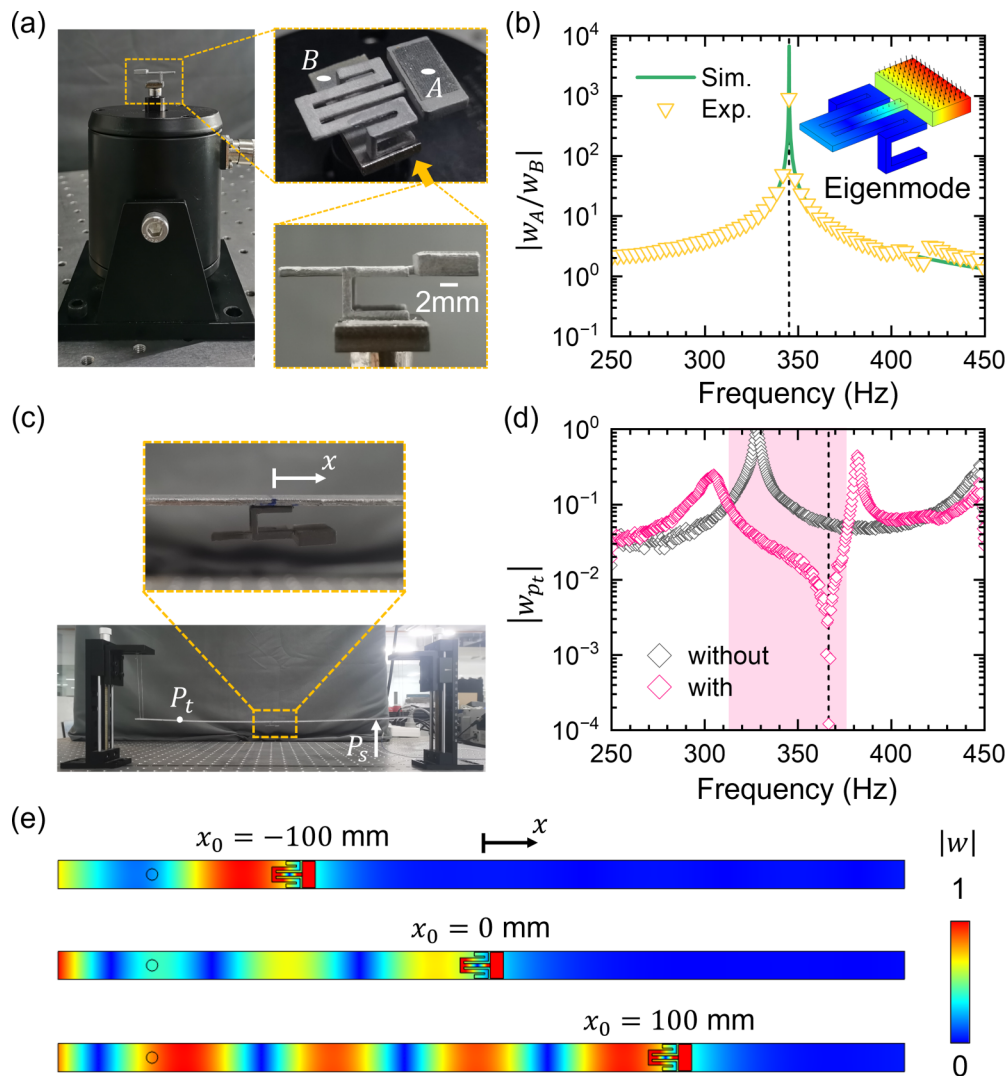


FIG. 1. A typical local resonator and isolating frequency shift of the corresponding meta-layer. (a) Eigenfrequency testing of the local resonator. The designed unit is fixed on a block (304 steel) and forced by a vibration exciter. (b) Experimental (yellow triangles) and numerical (green line) relative displacement versus excitation frequency.  $w_A$  and  $w_B$  refer to the displacements at points A (on the resonator) and B (on the block). Insert: Simulated eigenmode of the unit. (c) Isolation testing of the meta-layer fixed on an aluminum beam. Excitation is provided by a piezoelectric plate at point  $P_s$ . (d) Experimental frequency response.  $w_{p_t}$  is the displacement normalized by the max value at  $P_t$  with (pink) and without (gray) the resonator. (e) Simulated displacement fields of the unit located at  $x_0 = -100$  mm,  $x_0 = 0$  mm, and  $x_0 = 100$  mm at an isolating frequency  $f = 366.5$  Hz.

the resonator and the pedestal, respectively. Both numerical and experimental results indicate  $f_0 = 345.2$  Hz, with the corresponding eigenmode shown in the insert of Fig. 1(b). Then, we conducted further tests on the isolation performance of the locally resonant unit. The unit is fixed on an aluminum beam suspended by silk threads, as shown in Fig. 1(c). The beam is excited by a piezoelectric plate at point  $P_s$  ( $x = 175$  mm) and measured by a laser vibrometer at point  $P_t$  ( $x = -180$  mm). Additional details can be found in Supplemental Material Appendix S2 [42]. Experimental frequency responses are presented in Fig. 1(d), where the pink and gray rhombi represent the displacements (normalized by the max value) at  $P_t$  with and without the unit, respectively. The working frequency ranges from 312.7 to 376.5 Hz, which can be attributed to two factors: the alteration of eigenfrequency after pasting the unit and the local resonance of

the designed unit. The former splits one resonant peak into two peaks, while the latter results in an optimal isolation at  $f = 366.5$  Hz. Corresponding simulations of beams in Supplemental Material Appendix S3 [42] also indicate the existence of such a merit. It is stressed that the thickness of our layer is 23 mm, which is only  $\frac{1}{7}$  the wavelength at 366.5 Hz ( $\lambda = 158.7$  mm). Interestingly, when local resonators are monolayered rather than periodic in the direction of wave propagation, the bandgap is replaced by a perfectly isolating point ( $f = 366.5$  Hz) with a deviation of approximately 20 Hz from unit's eigenfrequency. Such a frequency shift will lead to a mismatch between engineering requirements and practical performance in vibration control, particularly in the low-frequency range. Therefore, it is imperative to investigate its underlying mechanism.

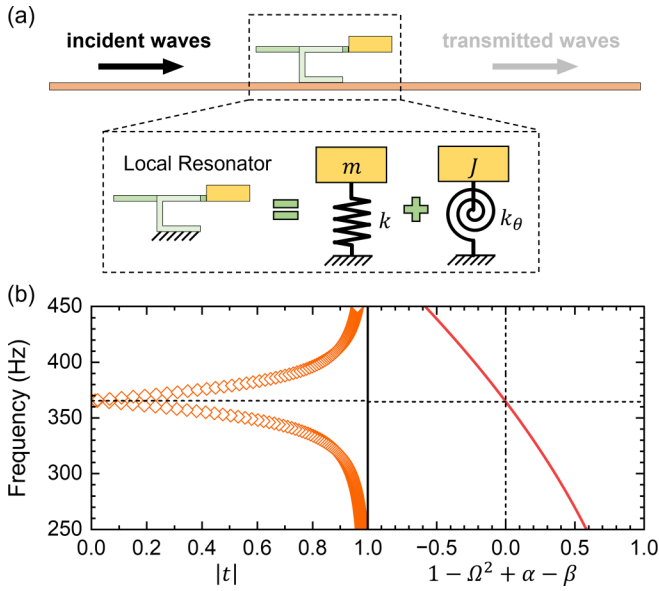


FIG. 2. Mechanism of the meta-layer for low-frequency isolation. (a) A schematic diagram of the locally resonant meta-layer. The designed unit is decoupled to mass-spring models of translation and rotation. (b) Simulated amplitude of transmission  $|t|$  (orange rhombi) and theoretical  $1 - \Omega^2 + \alpha - \beta$  (red line) are plotted as a function of frequency. Note that  $|t| = 0$  at  $f = 365.4$  Hz, which corresponds to  $f = 364.6$  Hz generated by  $1 - \Omega^2 + \alpha - \beta = 0$ .

To explore the mechanism of the isolating frequency shift, we simulate displacement fields of the unit located in different positions at 366.5 Hz, as shown in Fig. 1(e). Simulations of the meta-layer fixed on plates are also provided in Supplemental Material Appendix S4 [42]. The field patterns are obstructed by the locally resonant meta-layer, indicating that the local resonator functions as an obstacle rather than a dynamic vibration absorber. For a tiny and rigid obstacle, the mechanism of wave isolation has been investigated [35]. However, the deformation of the obstacle is non-negligible when local resonance is introduced. The designed unit is decoupled into mass-spring models of translation and rotation, as shown in Fig. 2(a).  $m$  and  $J$  represent the mass and moment of inertia of the block, while  $k$  and  $k_\theta$  denote the translational and rotational stiffness coefficients, respectively. Considering the continuity of the practical structure, it is reasonable to assume that the translational and rotational eigenfrequencies are equivalent ( $\omega_0 = \sqrt{k/m} = \sqrt{k_\theta/J}$ ). After detailed derivations (see Supplemental Material Appendix S4 [42]), it is determined that elastic waves are completely isolated (i.e., transmission  $|t| = 0$ ) when the locally resonant meta-layer satisfies

$$1 - \Omega^2 + \alpha - \beta = 0, \quad (1)$$

where  $\Omega = \omega/\omega_0$  is the frequency ratio between the angular frequency  $\omega$  of incident waves and the eigenfrequency  $\omega_0$  of units.  $\alpha = \frac{m\omega^2}{4EI\kappa^3}$  and  $\beta = \frac{J\omega^2}{4EI\kappa}$  are relative dynamic stiffnesses as resistances against translational and rotational motions, respectively, where  $\kappa$  is the wave number and  $EI$  is the bending stiffness of beams. Explicit formulas of  $m$  and  $J$  for specific units are provided in Supplemental Material Appendix S4 [42]. Equation (1) not only implies that the meta-layer

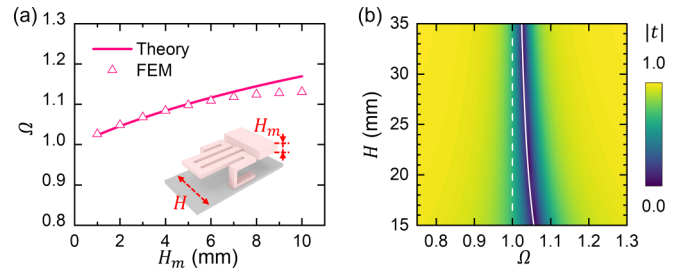


FIG. 3. Verification of the isolating frequency shift. (a) Theoretical ratio of isolating frequency and eigenfrequency  $\Omega$  (pink line) is plotted as functions of  $H_m$ . Pink triangles refer to  $\Omega$  provided by FEM. (b) Simulated transmission  $|t|$  is plotted as a function of frequency and  $H$ . The dashed and solid lines represent eigenfrequency and theoretical frequencies of  $|t| = 0$ , respectively.

functions through the coherent elimination of scattered and incident waves, but also demonstrates that the wave isolation by tiny and rigid obstacles [35] is a special case of  $\Omega$  approaching zero (namely,  $\omega_0 \rightarrow \infty$ ). Then, we verify Eq. (1) using the finite element method (FEM). The simulated transmission  $|t|$  is shown in Fig. 2(b), where  $|t|$  reaches zero ( $|t| = 0.004$ ) at  $f = 365.4$  Hz, coincident with the experimentally isolating frequency. We theoretically calculate  $1 - \Omega^2 + \alpha - \beta$  changing with incident frequency, as shown by the red curve in Fig. 2(b). The theoretically isolating frequency is  $f = 364.6$  Hz, which is only 0.2% less than the simulated frequency of  $|t| = 0$ . Such a consistency confirms that the isolation of the meta-layer is due to the total reflection of elastic waves. Simultaneously, it is also proved that the isolating frequency shift relative to eigenfrequency is an inherent property of single-layer structures and fundamentally distinct from bandgap-based metamaterials. We also present theoretical and numerical results of the meta-layer with different configurations in Supplemental Material Appendix S5 [42] to demonstrate the universality of the proposed method.

According to Eq. (1), the isolating frequency shift can be quantitatively obtained by  $\Omega = \sqrt{1 + \alpha - \beta}$ . It is evident that  $\Omega$  is controlled by  $\alpha$  and  $\beta$ , with the translational mode ( $\alpha$ ) increasing the isolating frequency and the rotational mode ( $\beta$ ) decreasing it. We then calculate  $\Omega$  changing with  $H_m$ , as shown in Fig. 3(a), where the theoretical  $\Omega$  is only 3.4% higher than the simulated result at  $H_m = 10$  mm. It is reasonable that the simulated  $\Omega$  becomes lower than the theoretical curve as  $H_m$  increases, because the practical rotation center deviates from the theoretical axis, which results in the increase of  $\beta$  and the decrease of  $\Omega$ . Additionally, simulated transmission  $|t|$  is also plotted as a function of the width of the beam  $H$  and the ratio of frequency of incident waves and eigenfrequency [Fig. 3(b)]. The region of  $|t| = 0$  deviates significantly from the eigenfrequency (dashed line), but is accurately predicted by the theory (solid line). The discussion of  $H_m$  and  $H$  justifies our theory from both the unit and the beam. More importantly, it confirms that the isolating frequency shift is induced by the coupling between the local resonator and the beam.

It should be noted that although the isolating frequency shift has been discovered [43,44], the proposed theory offers greater accuracy because of the inclusion of the rotational

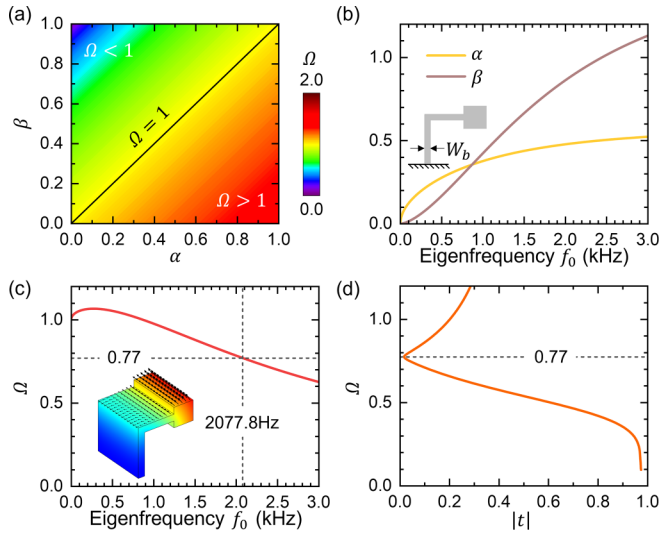


FIG. 4. A meta-layer with opposite-frequency shift. (a) Density map of the ratio of isolating frequency and eigenfrequency  $\Omega$  with respect to  $\alpha$  and  $\beta$ .  $\Omega = 1$  when  $\alpha = \beta$  (black line). (b) Theoretical  $\alpha$  and  $\beta$  change with eigenfrequency  $f_0$  of the designed unit to isolate flexural waves completely. (c) Corresponding  $\Omega$  is plotted as a function of  $f_0$ .  $\Omega = 0.77$  at  $f_0 = 2077.8$  Hz. (d) Simulated transmission  $|t|$  of the corresponding unit versus  $\Omega$ .  $|t| = 0$  at  $\Omega = 0.77$ , which agrees with the theoretical result.

mode ( $\beta$ ). Furthermore,  $\beta$  allows the isolating frequency to shift in an opposite direction, which is almost impossible in the single-mode theory. Figure 4(a) is the density map of  $\Omega$  with respect to  $\alpha$  and  $\beta$ , which is partitioned by a black line ( $\Omega = 1$  when  $\alpha = \beta$ ). We observe that  $\Omega < 1$  when  $\alpha < \beta$ , which indicates that the isolating frequency can be shifted not only to high frequency, but also to low frequency. To illustrate the arbitrariness and designability of the isolating frequency shift, we further design a new meta-layer consisting of a block and two beams, as shown in Fig. 4(b), to achieve the low-frequency shift. For convenience, we solely regulate the unit's eigenfrequency  $f_0$  while keeping its mass  $m$  and moment of inertia  $J$  constant. Corresponding materials and geometric

parameters are provided in Supplemental Material Appendix S5 [42]. The theoretical curve of  $\alpha$  and  $\beta$  with respect to  $f_0$  is shown in Fig. 4(b), where  $\alpha$  and  $\beta$  intersect at  $f_0 = 869.1$  Hz. When  $f_0 > 869.1$  Hz,  $\beta$  exceeds  $\alpha$ , resulting in the isolating frequency less than the eigenfrequency. Theoretical  $\Omega$  is further calculated as a function of  $f_0$  in Fig. 4(c), where  $\Omega < 1$  when  $f_0 > 869.1$  Hz. We select a unit with  $f_0 = 2077.1$  Hz as an example to verify the prediction by FEM. Here, we change the eigenfrequency of the unit by designing the width  $W_d$ . The eigenmode of the corresponding unit is shown in the insert to Fig. 4(c). After some simulations, transmission  $|t|$  is plot as a function of the ratio of incident wave frequency to eigenfrequency in Fig. 4(d). As expected,  $|t|$  is close to zero ( $|t| = 0.02$ ) when  $\Omega$  equals 0.77, which aligns precisely with the theoretical result. Therefore, we demonstrate that the elusive isolating frequency shift in locally resonant meta-layers can be explicated by the proposed theory. We also provide two more examples with the opposite-frequency shift effect in Supplemental Material Appendix S5 [42] to display the universality of our theory.

In summary, we design a locally resonant meta-layer achieving isolation of low-frequency elastic waves. The experimental results show that the monolayer structure of local resonators has an isolating frequency shift compared to its own eigenfrequency, which is a significant difference from metamaterials. We demonstrate theoretically that such a frequency shift is caused by the coupling between the unit and the beam. The theoretically isolating frequency is in good agreement with experimental and simulated results. In addition, we predict and simulate a meta-layer that can inversely reduce the isolating frequency, further proving the correctness of the proposed theory. The locally resonant meta-layer and corresponding theory provide a compact configuration and more accurate design guidance for vibration control.

This work was supported by the National Natural Science Foundation of China (Grants No. 12172271 and No. 12172041), the Open Project of the National Key Laboratory of Science and Technology on Liquid Rocket Engines (Grant No. 6142704220403), and the National Key Research and Development Program of China (Grant No. 2021YFF0500300).

- [1] D. J. Mead, *Passive Vibration Control* (John Wiley & Sons Ltd., Chichester, 1999).
- [2] J. L. Rose, *Ultrasonic Guided Waves in Solid Media* (Cambridge University Press, Cambridge, 2014).
- [3] R. Zhu, X. N. Liu, G. K. Hu, C. T. Sun, and G. L. Huang, Negative refraction of elastic waves at the deep-subwavelength scale in a single-phase metamaterial, *Nat. Commun.* **5**, 5510 (2014).
- [4] D. Tallarico, N. V. Movchan, A. B. Movchan, and D. J. Colquitt, Tilted resonators in a triangular elastic lattice: Chirality, Bloch waves and negative refraction, *J. Mech. Phys. Solids* **103**, 236 (2017).
- [5] H. Huang, S. Huo, and J. Chen, Subwavelength elastic topological negative refraction in ternary locally resonant phononic crystals, *Int. J. Mech. Sci.* **198**, 106391 (2021).
- [6] F. Liu and Z. Liu, Elastic waves scattering without conversion in metamaterials with simultaneous zero indices for longitudinal and transverse waves, *Phys. Rev. Lett.* **115**, 175502 (2015).
- [7] H. Dong, S. Zhao, Y. Wang, and C. Zhang, Topology optimization of anisotropic broadband double-negative elastic metamaterials, *J. Mech. Phys. Solids* **105**, 54 (2017).
- [8] S. H. Mousavi, A. B. Khanikaev, and Z. Wang, Topologically protected elastic waves in phononic metamaterials, *Nat. Commun.* **6**, 8682 (2015).
- [9] S. Yu, C. He, Z. Wang, F. Liu, X. Sun, Z. Li, H. Lu, M. Lu, X. Liu, and Y. Chen, Elastic pseudospin transport for integratable topological phononic circuits, *Nat. Commun.* **9**, 3072 (2018).
- [10] Z. Y. Liu, X. X. Zhang, Y. W. Mao, Y. Y. Zhu, Z. Y. Yang, C. T. Chan, and P. Sheng, Locally resonant sonic materials, *Science* **289**, 1734 (2000).

- [11] Z. Liu, C. T. Chan, and P. Sheng, Analytic model of phononic crystals with local resonances, *Phys. Rev. B* **71**, 014103 (2005).
- [12] H. H. Huang, C. T. Sun, and G. L. Huang, On the negative effective mass density in acoustic metamaterials, *Int. J. Eng. Sci.* **47**, 610 (2009).
- [13] X. Zhou and G. Hu, Analytic model of elastic metamaterials with local resonances, *Phys. Rev. B* **79**, 195109 (2009).
- [14] S. Yao, X. Zhou, and G. Hu, Experimental study on negative effective mass in a 1D mass–spring system, *New J. Phys.* **10**, 043020 (2008).
- [15] K. Chuang, X. Lv, and D. Wang, A tunable elastic metamaterial beam with flat-curved shape memory alloy resonators, *Appl. Phys. Lett.* **114**, 051903 (2019).
- [16] W. Gao, B. Yang, Y. Hong, K. Guo, P. Sun, and J. Sun, Investigation on tunable low-frequency property of magnetic field induced phononic crystal with Archimedean spiral-beams, *Mech. Syst. Signal Process.* **185**, 109756 (2023).
- [17] Z. Wang, Q. Zhang, K. Zhang, and G. Hu, Tunable digital metamaterial for broadband vibration isolation at low frequency, *Adv. Mater.* **28**, 9857 (2016).
- [18] Q. Lin, J. Zhou, K. Wang, D. Xu, G. Wen, Q. Wang, and C. Cai, Low-frequency locally resonant band gap of the two-dimensional quasi-zero-stiffness metamaterials, *Int. J. Mech. Sci.* **222**, 107230 (2022).
- [19] N. Yu, P. Genevet, M. A. Kats, F. Aieta, J. Tetienne, F. Capasso, and Z. Gaburro, Light propagation with phase discontinuities: Generalized laws of reflection and refraction, *Science* **334**, 333 (2011).
- [20] C. Pfeiffer and A. Grbic, Metamaterial Huygens’ surfaces: Tailoring wave fronts with reflectionless sheets, *Phys. Rev. Lett.* **110**, 197401 (2013).
- [21] H. Zhu and F. Semperlotti, Anomalous refraction of acoustic guided waves in solids with geometrically tapered metasurfaces, *Phys. Rev. Lett.* **117**, 034302 (2016).
- [22] J. Rong, W. Ye, S. Zhang, and Y. Liu, Frequency-coded passive multifunctional elastic metasurfaces, *Adv. Funct. Mater.* **30**, 2005285 (2020).
- [23] Y. Chen, X. Li, G. Hu, M. R. Haberman, and G. Huang, An active mechanical Willis meta-layer with asymmetric polarizabilities, *Nat. Commun.* **11**, 3681 (2020).
- [24] Q. Wu, X. Zhang, P. Shivashankar, Y. Chen, and G. Huang, Independent flexural wave frequency conversion by a linear active metalayer, *Phys. Rev. Lett.* **128**, 244301 (2022).
- [25] H. Lee, J. K. Lee, H. M. Seung, and Y. Y. Kim, Mass-stiffness substructuring of an elastic metasurface for full transmission beam steering, *J. Mech. Phys. Solids* **112**, 577 (2018).
- [26] Y. Jin, W. Wang, A. Khelif, and B. Djafari-Rouhani, Elastic metasurfaces for deep and robust subwavelength focusing and imaging, *Phys. Rev. Appl.* **15**, 024005 (2021).
- [27] S. Yuan, A. Chen, X. Du, H. Zhang, B. Assouar, and Y. Wang, Reconfigurable flexural waves manipulation by broadband elastic metasurface, *Mech. Syst. Signal Process.* **179**, 109371 (2022).
- [28] Y. Liu, Z. Liang, F. Liu, O. Diba, A. Lamb, and J. Li, Source illusion devices for flexural lamb waves using elastic metasurfaces, *Phys. Rev. Lett.* **119**, 034301 (2017).
- [29] S. Li, J. Xu, and J. Tang, Tunable modulation of refracted lamb wave front facilitated by adaptive elastic metasurfaces, *Appl. Phys. Lett.* **112**, 021903 (2018).
- [30] B. Li, Y. Hu, J. Chen, G. Su, Y. Liu, M. Zhao, and Z. Li, Efficient asymmetric transmission of elastic waves in thin plates with lossless metasurfaces, *Phys. Rev. Appl.* **14**, 054029 (2020).
- [31] L. Cao, Y. Xu, B. Assouar, and Z. Yang, Asymmetric flexural wave transmission based on dual-layer elastic gradient metasurfaces, *Appl. Phys. Lett.* **113**, 183506 (2018).
- [32] Y. Xie, W. Wang, H. Chen, A. Konneker, B. Popa, and S. A. Cummer, Wavefront modulation and subwavelength diffractive acoustics with an acoustic metasurface, *Nat. Commun.* **5**, 5553 (2014).
- [33] H. Zhu, S. Patnaik, T. F. Walsh, B. H. Jared, and F. Semperlotti, Nonlocal elastic metasurfaces: Enabling broadband wave control via intentional nonlocality, *Proc. Natl. Acad. Sci. USA* **117**, 26099 (2020).
- [34] Y. Hu, Y. Zhang, G. Su, M. Zhao, B. Li, Y. Liu, and Z. Li, Realization of ultrathin waveguides by elastic metagratings, *Commun. Phys.* **5**, 62 (2022).
- [35] Y. Zhang, Z. Sha, G. Su, H. Zhou, X. Zhang, Y. Liu, B. Li, and T. Wang, Meta-fences for flexural waves in plates, *Extreme Mech. Lett.* **52**, 101659 (2022).
- [36] G. Ma, M. Yang, S. Xiao, Z. Yang, and P. Sheng, Acoustic metasurface with hybrid resonances, *Nat. Mater.* **13**, 873 (2014).
- [37] X. Fang, J. Wen, B. Bonello, J. Yin, and D. Yu, Ultra-low and ultra-broad-band nonlinear acoustic metamaterials, *Nat. Commun.* **8**, 1288 (2017).
- [38] L. Li, L. Tan, L. Kong, D. Wang, and H. Yang, The influence of flywheel micro vibration on space camera and vibration suppression, *Mech. Syst. Signal Process.* **100**, 360 (2018).
- [39] H. Oh, K. Lee, and M. Jo, A passive launch and on-orbit vibration isolation system for the spaceborne cryocooler, *Aerosp. Sci. Technol.* **28**, 324 (2013).
- [40] E. Baravelli and M. Ruzzene, Internally resonating lattices for bandgap generation and low-frequency vibration control, *J. Sound. Vib.* **332**, 6562 (2013).
- [41] L. Cao, Y. Zhu, S. Wan, Y. Zeng, and B. Assouar, On the design of non-Hermitian elastic metamaterial for broadband perfect absorbers, *Int. J. Eng. Sci.* **181**, 103768 (2022).
- [42] See Supplemental Material at <http://link.aps.org/supplemental/10.1103/PhysRevB.108.L140303> for detailed experimental setup, results, and analysis.
- [43] M. J. Brennan, Control of flexural waves on a beam using a tunable vibration neutralizer, *J. Sound Vib.* **222**, 389 (1998).
- [44] H. M. El-Khatib, B. R. Mace, and M. J. Brennan, Suppression of bending waves in a beam using a tuned vibration absorber, *J. Sound Vib.* **288**, 1157 (2005).